Geochemical Perspectives Letters

Expanding time-temperature chronometry for arc magmas with MgO diffusion in hydrous melts

O. Callejas[1*], M. Holycross[1], E. Gazel[1], E.G. Huggins[1]

https://doi.org/10.7185/geochemlet.2541

Abstract

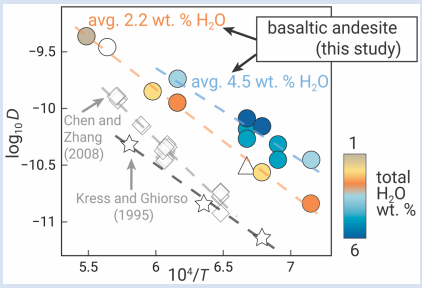

The diffusion of MgO in olivine hosted melt inclusions is a geochemical chronometer that can effectively quantify magma cooling rates and track the thermal histories of volcanic eruptions. MgO diffusion in dry silicate melts has been experimentally measured, but the currently available data are insufficient to provide an accurate assessment of model time-temperature processes in H_2O-bearing magmas. Here, we conducted piston cylinder experiments ($T = 1125$–1550 °C, $P = 1$ GPa, and varying dissolved H_2O contents) to constrain MgO diffusivities during olivine dissolution in a hydrous basaltic andesite melt. We calculated diffusion coefficients for MgO (D_{MgO}) using a semi-infinite solution approach and forward modelling. D_{MgO} showed two congruent Arrhenius relationships at average ~2.2 and ~4.5 wt. % dissolved H_2O, with D_{MgO} increasing linearly as more dissolved water was added at constant temperature. The applications of our new, internally consistent data set of MgO diffusivities will improve models that seek to understand minute-to-hour timescales and derive thermal histories recorded by arc magmatic systems.

Received 21 May 2025 | Accepted 29 August 2025 | Published 27 October 2025

Introduction

Quantifying the syn-eruptive *pressure-temperature-time* pathways of magmas is critical for understanding the magmatic drivers of eruption intensity and behaviour. Melt inclusions (MIs) are useful to directly access magmatic conditions at the time of entrapment; however, post-entrapment crystallisation processes may complicate the reconstruction of initial melt compositions and volatile contents (*e.g.*, Danyushevsky *et al.*, 2000; Gaetani and Watson, 2000). Previous studies have addressed this by applying bulk corrections under the assumption of chemical homogeneity (*e.g.*, Danyushevsky *et al.*, 2000; Gaetani and Watson, 2000) but are limited in resolving internal compositional gradients. In contrast, chemical zonation profiles in olivine hosted MIs provide practical advantages to study the systematics of various magmatic settings on Earth (*e.g.*, Watson and Baker, 1991; Costa and Chakraborty, 2004; Newcombe *et al.*, 2014, 2020; Costa *et al.*, 2020; Wallace *et al.*, 2021) and Mars (*e.g.*, Saper and Stolper, 2020) because they record the diffusion of MgO in the silicate melt during post-entrapment crystallisation of olivine on MIs walls. The resulting concentration gradients can be leveraged as a powerful chronometer for quantifying the timescales of magma ascent and other relatively rapid volcanic processes (*e.g.*, Newcombe *et al.*, 2014, 2020; Saper and Stolper, 2020). Calibrating MgO diffusion provides a unique opportunity to expand the chronometry recorded by Fe-Mg exchange (Dohmen *et al.*, 2007) and H^+ diffusion in olivine (Barth *et al.*, 2019) because (1) it can track temperature sensitive changes over periods of minutes-to-hours, and (2) it is not orientation dependent. Additionally, MgO profiles in silicate melts can be measured using commonly available analytical equipment (EPMA, SEM-EDS), thus facilitating quick and cost effective data collection.

Widespread application of this innovative approach is currently limited by a lack of MgO diffusion data for hydrous melt compositions. MgO diffusion during olivine dissolution has been experimentally calibrated in nominally anhydrous (0.25–0.4 wt. % H_2O) mid-ocean ridge basaltic melts (Chen and Zhang, 2008). Newcombe *et al.* (2014, 2020) have investigated chemical gradients in olivine hosted MIs from ocean island and arc volcanoes by applying the data set of Chen and Zhang (2008) to calculate cooling rates and track the thermal histories of volcanic eruptions. However, Arrhenius relationships for MgO diffusion have only been established for dry basaltic melts. The use of dry melt data to estimate the thermal histories of H_2O-bearing magmas is not entirely appropriate because the presence of dissolved H_2O enhances diffusion rates (*e.g.*, Watson, 1981), resulting in rapidly increased diffusivity as more dissolved water is incorporated into the melt. Consequently, applications of dry D_{MgO} will yield erroneously long timescales for modelled volcanic processes in hydrous systems.

To account for the effects of H_2O on MgO diffusion, Newcombe *et al.* (2020) conducted one additional experiment using a hydrous basaltic andesite melt at 1225 °C and 1 GPa. But aside from this single D_{MgO} measurement, no other MgO diffusion data in hydrous silicate melts have been published. This experimental study expands on the understanding of MgO diffusion in hydrous silicate melts by reporting an internally consistent data set at 1125–1550 °C and 2.2–4.5 wt. % H_2O. Our results can be applied to model the thermal histories

1. Department of Earth and Atmospheric Sciences, Cornell University, Ithaca, NY 14853, USA
* Corresponding author (email: oc68@cornell.edu, odalyscallejasg@gmail.com)

and eruptive styles of global arc magmas, which contain 4 wt. % H_2O on average, but span from 1–6 wt. % (Plank *et al.*, 2013). Our results may also be useful in evaluating post-entrapment processes (*e.g.*, cooling, decompression, crystallisation) that lead to vapour bubble growth in MIs (Rasmussen *et al.*, 2020). Finally, because MgO diffusion in the melt is considered to be the rate limiting step for olivine growth and dissolution (Chen and Zhang, 2008), accurate measurements of MgO diffusion in melts of varying composition are essential for quantifying kinetic controls on olivine saturation in magmas.

Experimental and Analytical Techniques

We conducted series of piston cylinder experiments in the experimental geochemistry lab at Cornell University following the approach of Chen and Zhang (2008). San Carlos Olivine (SCO; Fo_{90}) grains were: cored into 2.5 mm diameter rods, sliced into 0.3–0.5 mm thick discs, manually grounded with progressively finer SiC paper; then machine polished with alumina suspension and subsequently with colloidal silica to remove near surface crystal defects (following the methodology of Watson *et al.*, 2016). We examined each disc under a petrographic microscope to ensure these were inclusion- and crack-free (occasionally, crystals with small cracks that did not disturb the interface were deemed acceptable). We placed each SCO disc in a single (graphite only or $Au_{90}Pd_{10}$ only) or double (inner graphite liner + either Ni or $Au_{90}Pd_{10}$) capsule. We strategically selected the capsule materials to best preserve the original water content of the melt while simultaneously preventing capsule melting at high temperatures (Fig. S-1; see SI).

We used reagent grade powdered oxides to make two synthesised powder mixes (melt) of basaltic andesite composition (Table S-2) at initial ~4 wt. % and ~6 wt. % dissolved H_2O, respectively. All H_2O was added as $Al(OH)_3$. The powder mix was packed in the capsule, on top of the polished SCO. Each capsule was fit into a MgO pressure media, placed inside a graphite heater, and then into a ½″ $BaCO_3$ cell. We used similar capsule size and geometry for all experiments to optimise consistency at a given nominal temperature-pressure condition. The experiment temperatures spanned from 1125–1550 °C with variable times (Table S-1). The experimental assemblies were pressurised to 1 GPa. All samples were quenched by turning off the power. See SI for more details.

We mounted each sample in epoxy to expose and polish the experimental glass before chemical analysis. Major and minor element compositions of all experiments were measured by a Cameca SXFive electron microprobe (EPMA) at Syracuse University and/or a JSM-IT700HR scanning electron microscope at the Cornell Mass Spectrometry (CMaS) facilities in the Department of Earth and Atmospheric Sciences (EAS). Specific conditions and data collection routines used for each instrument are outlined in SI. A minimum of three glass

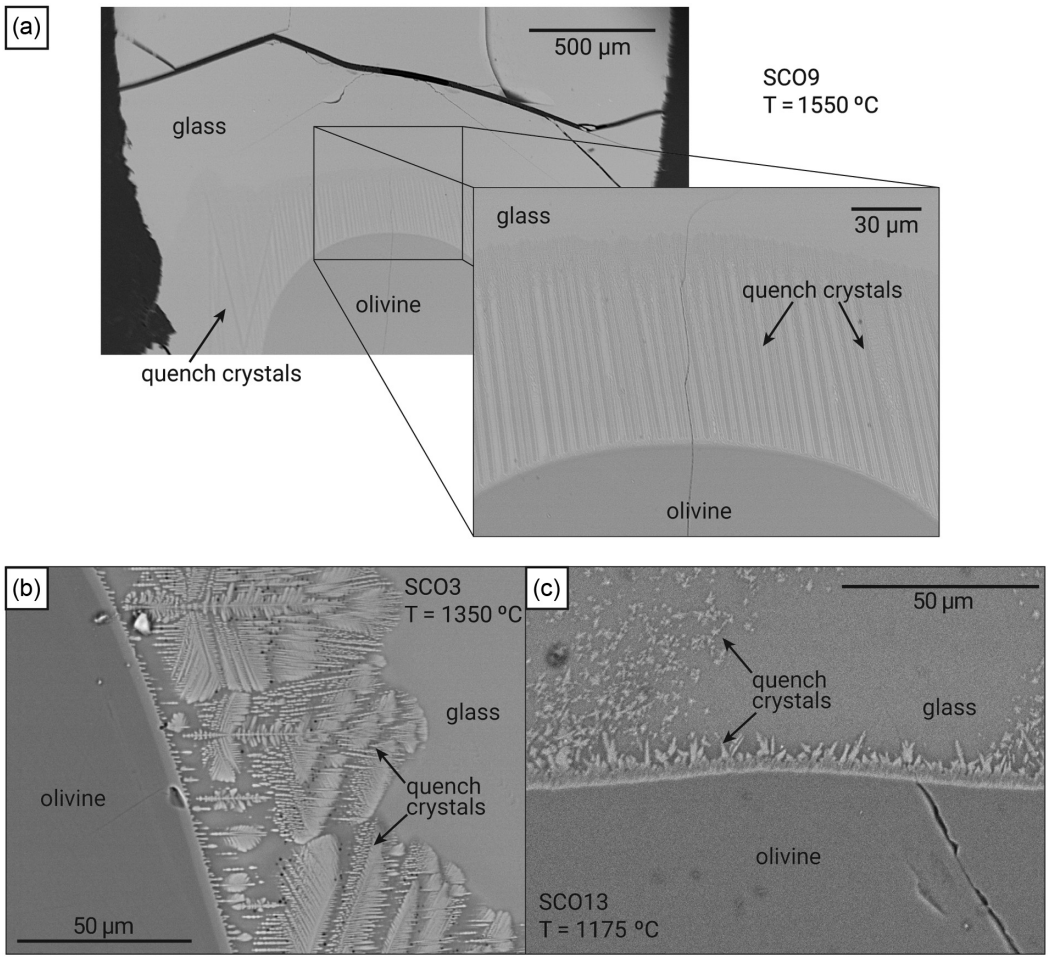

Figure 1 Examples of experiment textures. Decompression cracks are present in all experiments. Quench crystals are largest in high temperature experiments. **(a)** BSE image of SCO9 at 1550 °C. Zoomed in panel shows crystals at the olivine melt interface that formed upon quench. **(b)** BSE image of SCO3 at 1350 °C illustrating dendritic quench crystals near the interface. **(c)** BSE image of SCO13 at 1175 °C showing clusters of smaller quench crystals near the interface.

transects (Tables S-5 to S-18) were taken from the flat olivine melt interface towards the end of the capsule. Collecting multiple transects optimised the precision of our reported data and allowed us to determine if recovered MgO gradients could be due to mass transport or by a process other than diffusion. If multiple transects in one single experiment were inconsistent, we labelled them as "failed experiments" and omitted those results. Backscatter electron (BSE) images were captured to observe textures and measure olivine dissolution from the olivine interface into the melt (Fig. 1).

Samples were prepared for Fourier transform infrared (FTIR) spectroscopy measurements in the Department of EAS at Cornell University to quantify the dissolved H_2O content of each glass. Preparation included cutting thin wafers, grinding, and doubly polishing — following the methods of Dixon *et al.* (1995). See SI for specific instrument settings and procedures.

MgO concentration profiles were fitted using the ORIGIN™ software *via* the semi-infinite solution approach:

$$C(x,t) = C_s - \mathrm{erf}\left(\frac{x}{2\sqrt{D_{\mathrm{MgO}} \cdot t}}\right) \cdot (C_s - C_0) \qquad \text{Eq. 1}$$

where $C(x,t)$ is the concentration of MgO at a given distance (x) and time (t), C_0 is the concentration of MgO at the olivine melt interface, C_s is the initial MgO in the melt. The effective binary diffusivity of MgO, D_{MgO}, was calculated based on the known variables described above (Fig. 2). Error calculations are explained in SI. Experimental durations were corrected following effective time calculation methods from Zhang and Behrens (2000). An explicit finite difference method forward model was used to extract MgO diffusivities in five experiments that violated the infinite medium assumption. Measured MgO diffusivities were grouped by average of final dissolved water content (either ~2.2 or ~4.5 wt. %; Fig. 3) and fit with a linear regression to characterise the temperature dependence of diffusion according to the Arrhenius equation:

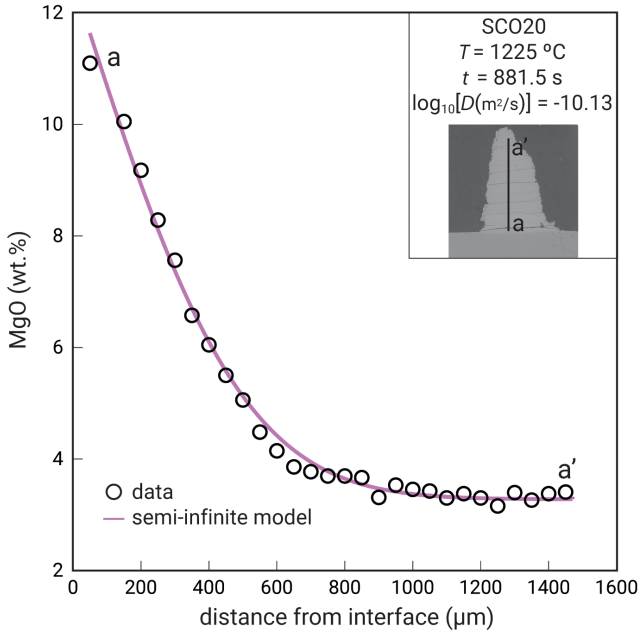

Figure 2 Diffusion profile and best fit. Measured MgO concentrations are shown as black circles. Coloured line corresponds to the semi-infinite model. Inset: BSE image for SCO20; black line shows location and direction (a to a') of one of three traverses on this sample.

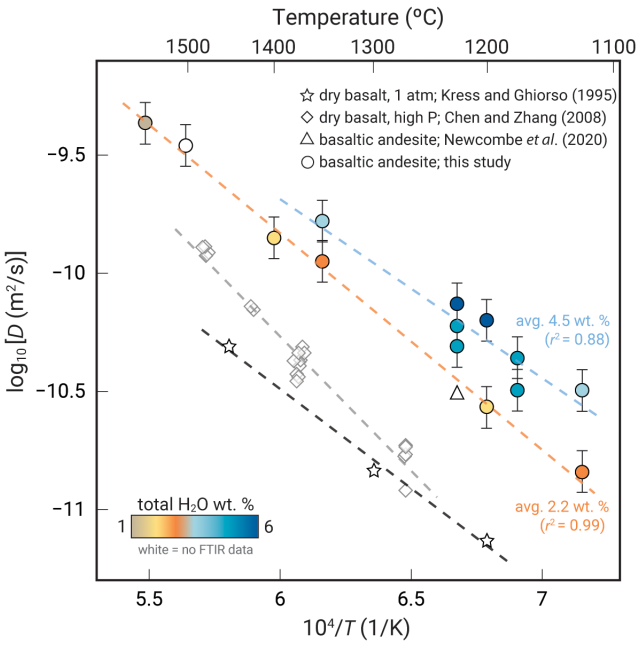

Figure 3 D_{MgO} as a function of T at ~2.2 and ~4.5 wt. % water at 1 GPa, compared to D_{MgO} in dry basalt at 1 atm (Kress and Ghiorso, 1995), dry MORB at 0.47–1.42 GPa (Chen and Zhang, 2008), and a hydrous D_{MgO} data point (Newcombe *et al.*, 2020). Colour gradient shows measured water *via* FTIR.

$$D = D_0 \cdot \exp\left(\frac{-E_a}{RT}\right) \qquad \text{Eq. 2}$$

where D_0 is the pre-exponential factor (m^2/s), E_a is the activation energy (J/mol), R is the gas constant (J/K·mol), and T is temperature (Kelvin).

Results

All SCO crystals showed some degree of dissolution during the experiment — initially flat crystals now show curvatures on the olivine edges, and quench crystals are present along the interface (Fig. 1). Decompression fractures were evident in the glass and olivine after all experimental runs. Analyses of quench crystals and decompression cracks in the glass were excluded from diffusion modelling to prevent data scatter in MgO diffusion profiles. Uphill diffusion was observed in the concentration profiles of CaO, Al_2O_3, and Na_2O; however, MgO exhibited no such behaviour and showed no other diffusion anomalies.

For experiments at 1175 °C to 1225 °C (Fig. 1c), the interface was minimally disturbed by the presence of quench crystals (individual size ≤10 μm). For experiments at 1350 °C (Fig. 1b), clusters of dendritic textures were observed up to 100 μm away from the interface. For experiments at >1400 °C (Fig. 1a), needle shaped crystals were observed near the interface and extended up to 200 μm into the glass. The observed textures and sizes of quench crystals were dependent on the experiment temperature, not the duration of the runs. This is in agreement with the findings of Chen and Zhang (2008), and indicates that the crystals formed during experiment cooling (quenching). Higher temperature experiments (Fig. 1a) were subject to greater degrees of quench crystal growth because, at constant quench rate, they take longer to cool below the glass transition.

The composition of these quench crystals could not be precisely measured *via* EPMA due to either their small size or

acicular aspect ratios (all analyses were subject to secondary fluorescence from the melt). Our limited analyses suggested that the quench crystals are primarily olivine and clinopyroxene. In most cases, the presence of quench crystals did not alter the preservation of the broad error function shape of the MgO diffusion profiles. However, in three experiments at 1400–1550 °C, olivine overgrowth did disturb the compositional profiles, so the transects were split into two: (1) from the interface to the end of the overgrowth, and (2) 10 µm away from the end of the overgrowth to the end of the capsule (crystal-free glass). Fitting of such profiles was performed by omitting the first segment and exclusively using the second one.

FTIR analyses revealed our experimental glasses largely did not retain their initial water contents of 4 or 6 wt. % (Table S-1, Fig. S-1). This was expected, as noble metals and graphite are not perfect containers for H_2O (or rather H_2; *e.g.*, Truckenbrodt and Johannes, 1999). To mitigate H_2O losses, we shortened the experiment run times and carefully selected capsule materials that were most effective at retaining H_2 whilst preventing capsule melting at intermediate and high temperatures (see SI).

The temperature dependence of MgO diffusion produced coherent Arrhenius relationships, which are grouped by average final dissolved water content of ~2.2 and ~4.5 wt. % (Fig. 3), and yielded distinct pre-exponential factors ($D_{0,\,2.2} = 4.04\text{E}{-}05 \pm 1.39\text{E}{-}05$ m^2/s and $D_{0,\,4.5} = 7.26\text{E}{-}06 \pm 5.73\text{E}{-}07$ m^2/s) and activation energy ($E_{a,\,2.2} = 173{,}255 \pm 4{,}891$ J/mol and $E_{a,\,4.5} = 143{,}977 \pm 21{,}681$ J/mol) (Table S-3). Grouping the MgO diffusion data by initial water content results in less congruent Arrhenius relationships for both groups (Fig. S-3). Additionally, we note that the datum of Newcombe *et al.* (2020) for MgO diffusion in a basaltic andesite melt of initial 3.8 wt. % H_2O plots along our ~2.2 wt. % Arrhenius relationship. Newcombe *et al.* (2020) did not determine the post-experiment concentration of H_2O in their melt, so it is possible that their sample did not maintain its initial H_2O content.

Discussion

Although our glasses did not retain their initial water contents, our results are highly relevant to natural diffusion scenarios where olivine growth occurs simultaneously with melt inclusion dehydration *via* H_2 diffusion in olivine (*e.g.*, Barth *et al.*, 2019). We interpret the final measured dissolved water content of the glass to be representative of the conditions in which the bulk of MgO diffusion occurred. This interpretation is supported by the low standard deviations of multiple FTIR measurements on glass collected at various locations throughout the capsule (Table S-1), which show water loss was relatively uniform throughout the capsule at the spatial resolution of FTIR. The diffusion of H_2O in melt is faster than the measured diffusion of MgO such that gradients in the chemical potential of H_2O in melt will be equilibrated much more rapidly than that of MgO. For instance, using the H_2O diffusivity parameterisation from Behrens *et al.* (2004), we calculate the H_2O diffusive length scale in experiment 21 using:

$$x = (D \cdot t)^{1/2} \qquad \text{Eq. 3}$$

and it resulted to be ~20 % longer than the MgO diffusive length scale at the same conditions.

Our measured D_{MgO} values at ~4.5 wt. % are roughly one order of magnitude higher than those reported in dry MORB at high pressures (Chen and Zhang, 2008) and up to two orders of magnitude higher than D_{MgO} in dry basalt at 1 atm (Kress and Ghiorso, 1995) (Fig. 3). Our results demonstrate that element diffusion rates in silicate melts are positively correlated with dissolved water content, in agreement with many other studies (*e.g.*, Mungall *et al.*, 1999; Holycross and Watson, 2018; Troch *et al.*, 2024). The positive relationship between element diffusivities in melt and dissolved water content is a result of melt depolymerisation — as H_2O dissociates, it reacts with bridging oxygen in the melt by rupturing Si-O-Si linkages and forming hydroxyl groups (Stolper, 1982).

Above ~3 wt. % dissolved H_2O, the function of $\log_{10}D$ and dissolved water content has previously shown to be asymptotic for most cations (Watson, 1981). That is, $\log_{10}D$ is dependent on the square root of dissolved water content, perhaps because the dissolution of molecular H_2O in a glass at that point has a negligible impact on viscosity. In contrast, our data is best fit by a linear relationship between $\log_{10}D_{MgO}$ and dissolved water in the melt (Fig. S-4). Linear relationships between measured D and dissolved H_2O are not uncommon and have been recorded for alkali diffusion in silicate melts (Watson, 1979; Troch *et al.*, 2024). Watson (1981) noted that diffusivities of very fast diffusing elements tend to be less inflated by the addition of dissolved water compared to slow diffusing elements, indicating there could be an upper limit to element diffusion speeds in melts. Zhang *et al.* (2010) also suggest that the $\log_{10}D$ of neutral species varies linearly with melt water content. This could explain our observations if Mg is transported through the melt as MgO. Finally, we note that our results (Fig. S-4) align with theoretical predictions and the literature (Watson, 1981; Mungall, 2002; Holycross *et al.*, 2018) by showing that as dissolved water content increases, the activation energy of MgO diffusion decreases.

The effects of H_2O on MgO diffusion can be parameterised using:

$$\ln D_{MgO} = \ln D_0 - \frac{E_a}{RT} + k \cdot H_2O \qquad \text{Eq. 4}$$

where D_{MgO} is the MgO diffusion coefficient (m^2/s), D_0 is the pre-exponential factor calculated as 1.89E−05 m^2/s (errors reported in Table S-3), the activation energy (E_a) is 167,674 ± 11,469 J/mol, R is the gas constant (J/K·mol), T is temperature (Kelvin), k is a coefficient that represents the observed linear relationship between $\log D_{MgO}$ and H_2O (Fig. S-4) and is calculated as 0.19 ± 0.06, and H_2O is the measured water content in the melt (wt. %). Equation 4 is strongly supported by our dataset ($r^2 = 0.98$) and enables reliable calculation of MgO diffusivity across a range of temperatures and varying H_2O contents in basaltic andesite melts.

Implications

The diffusion of MgO in hydrous basaltic andesite will bracket the magmatic histories recorded by Fe-Mg exchange (Dohmen *et al.*, 2007; Shea *et al.*, 2023) and H^+ diffusion in olivine (Barth *et al.*, 2019) (Fig. 4). MgO diffusion chronometry is uniquely poised to unlock community knowledge of magma ascent rates and the timescales of other syn-eruptive volcanic processes (Newcombe *et al.*, 2014, 2020; Saper and Stolper, 2020) because it is not orientation dependent and its diffusion behaviour appears to be relatively simple compared to other crystalline chronometers (*e.g.*, Barth *et al.*, 2023). Our newly reported MgO diffusion coefficients show that dissolved water in melt exerts direct control on the speed of MgO transport during olivine growth or dissolution. For example, application of the dry D_{MgO} diffusion data of Chen and Zhang (2008) to a 20 µm MgO diffusion profile produced at 1100 °C yields a diffusive timescale of 3.6 min using Equation 3. Application of our new hydrous (~4.5 wt. % H_2O) data to this same profile will return

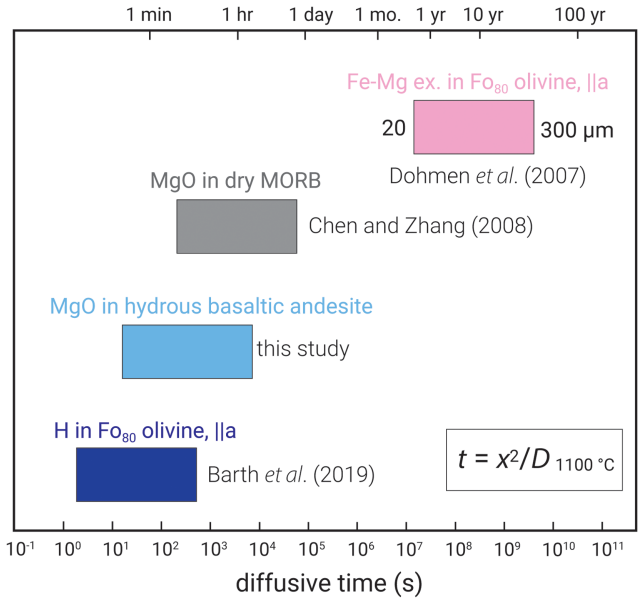

Figure 4 Timescales recorded by diffusion chronometers for mafic arc systems including Fe-Mg exchange in Fo_{80} (Dohmen *et al.*, 2007), MgO in dry MORB (Chen and Zhang, 2008), D_{MgO} in hydrous basaltic andesite (this study, covering diffusivities at 2.2 and 4.5 wt. % H_2O), and H in Fo_{80} olivine (Barth *et al.*, 2019). Timescales were modelled using inset equation with $x = 20$–300 µm and D was calculated at 1100 °C.

a timescale of 18 s, nearly an order of magnitude shorter (Fig. 4). Hence, the effect of water on D_{MgO} must not be overlooked; otherwise, it will lead to inaccurate calculations of the timescales associated with arc magmatic events.

Acknowledgements

We are grateful to K. Dayton for analytical help and B. Garvey for programming insight. This manuscript benefitted from feedback by M. Newcombe, an anonymous reviewer, and R. Fonseca (editor). This study was supported by Cornell University start up funds to MH.

Editor: Raul O.C. Fonseca

Additional Information

Supplementary Information accompanies this letter at https://www.geochemicalperspectivesletters.org/article2541.

Cite this letter as: Callejas, O., Holycross, M., Gazel, E., Huggins, E.G. (2025) Expanding time-temperature chronometry for arc magmas with MgO diffusion in hydrous melts. *Geochem. Persp. Let.* 37, 24–29. https://doi.org/10.7185/geochemlet.2541

References

Barth, A., Newcombe, M., Plank, T., Gonnermann, H., Hajimirza, S., Soto, G.J., Saballos, A., Hauri, E. (2019) Magma decompression rate correlates with explosivity at basaltic volcanoes — Constraints from water diffusion in olivine. *Journal of Volcanology and Geothermal Research* 387, 106664. https://doi.org/10.1016/j.jvolgeores.2019.106664

Barth, A., Plank, T., Towbin, H. (2023) Rates of dehydration in hydrous, high-Fo, magmatic olivines. *Geochimica et Cosmochimica Acta* 342, 62–73. https://doi.org/10.1016/j.gca.2022.11.009

Behrens, H., Zhang, Y., Xu, Z. (2004) H_2O diffusion in dacitic and andesitic melts. *Geochimica et Cosmochimica Acta* 68, 5139–5150. https://doi.org/10.1016/j.gca.2004.07.008

Chen, Y., Zhang, Y. (2008) Olivine dissolution in basaltic melt. *Geochimica et Cosmochimica Acta* 72, 4756–4777. https://doi.org/10.1016/j.gca.2008.07.014

Costa, F., Chakraborty, S. (2004) Decadal time gaps between mafic intrusion and silicic eruption obtained from chemical zoning patterns in olivine. *Earth and Planetary Science Letters* 227, 517–530. https://doi.org/10.1016/j.epsl.2004.08.011

Costa, F., Shea, T., Ubide, T. (2020) Diffusion chronometry and the timescales of magmatic processes. *Nature Reviews Earth & Environment* 1, 201–214. https://doi.org/10.1038/s43017-020-0038-x

Danyushevsky, L.V., Della-Pasqua, F.N., Sokolov, S. (2000) Re-equilibration of melt inclusions trapped by magnesian olivine phenocrysts from subduction-related magmas: petrological implications. *Contributions to Mineralogy and Petrology* 138, 68–83. https://doi.org/10.1007/PL00007664

Dixon, J.E., Stolper, E.M., Holloway, J.R. (1995) An Experimental Study of Water and Carbon Dioxide Solubilities in Mid-Ocean Ridge Basaltic Liquids. Part I: Calibration and Solubility Models. *Journal of Petrology* 36, 1607–1631. https://doi.org/10.1093/oxfordjournals.petrology.a037267

Dohmen, R., Becker, H.-W., Chakraborty, S. (2007) Fe–Mg diffusion in olivine I: experimental determination between 700 and 1,200°C as a function of composition, crystal orientation and oxygen fugacity. *Physics and Chemistry of Minerals* 34, 389–407. https://doi.org/10.1007/s00269-007-0157-7

Gaetani, G.A., Watson, E.B. (2000) Open system behavior of olivine-hosted melt inclusions. *Earth and Planetary Science Letters* 183, 27–41. https://doi.org/10.1016/S0012-821X(00)00260-0

Holycross, M.E., Watson, E.B. (2018) Trace element diffusion and kinetic fractionation in wet rhyolitic melt. *Geochimica et Cosmochimica Acta* 232, 14–29. https://doi.org/10.1016/j.gca.2018.04.006

Holycross, M.E., Watson, E.B., Richter, F.M., Villeneuve, J. (2018) Diffusive fractionation of Li isotopes in wet, highly silicic melts. *Geochemical Perspectives Letters* 6, 39–42. https://doi.org/10.7185/geochemlet.1807

Kress, V.C., Ghiorso, M.S. (1995) Multicomponent diffusion in basaltic melts. *Geochimica et Cosmochimica Acta* 59, 313–324. https://doi.org/10.1016/0016-7037(94)00286-U

Mungall, J.E. (2002) Empirical models relating viscosity and tracer diffusion in magmatic silicate melts. *Geochimica et Cosmochimica Acta* 66, 125–143. https://doi.org/10.1016/S0016-7037(01)00736-0

Mungall, J.E., Dingwell, D.B., Chaussidon, M. (1999) Chemical diffusivities of 18 trace elements in granitoid melts. *Geochimica et Cosmochimica Acta* 63, 2599–2610. https://doi.org/10.1016/S0016-7037(99)00209-4

Newcombe, M.E., Fabbrizio, A., Zhang, Y., Ma, C., Le Voyer, M., Guan, Y., Eiler, J.M., Saal, A.E., Stolper, E.M. (2014) Chemical zonation in olivine-hosted melt inclusions. *Contributions to Mineralogy and Petrology* 168, 1030. https://doi.org/10.1007/s00410-014-1030-6

Newcombe, M.E., Plank, T., Zhang, Y., Holycross, M., Barth, A., Lloyd, A.S., Ferguson, D., Houghton, B.F., Hauri, E. (2020) Magma Pressure-Temperature-Time Paths During Mafic Explosive Eruptions. *Frontiers in Earth Science* 8, 531911. https://doi.org/10.3389/feart.2020.531911

Plank, T., Kelley, K.A., Zimmer, M.M., Hauri, E.H., Wallace, P.J. (2013) Why do mafic arc magmas contain ~4 wt% water on average? *Earth and Planetary Science Letters* 364, 168–179. https://doi.org/10.1016/j.epsl.2012.11.044

Rasmussen, D.J., Plank, T.A., Wallace, P.J., Newcombe, M.E., Lowenstern, J.B. (2020) Vapor-bubble growth in olivine-hosted melt inclusions. *American Mineralogist* 105, 1898–1919. https://doi.org/10.2138/am-2020-7377

Saper, L.M., Stolper, E.M. (2020) Controlled Cooling-Rate Experiments on Olivine-Hosted Melt Inclusions: Chemical Diffusion and Quantification of Eruptive Cooling Rates on Hawaii and Mars. *Geochemistry, Geophysics, Geosystems* 21, e2019GC008772. https://doi.org/10.1029/2019GC008772

Shea, T., Ruth, D., Jollands, M., Ohtaki, K., Ishii, H., Bradley, J. (2023) The presence of silicate melt may enhance rates of cation diffusion in olivine. *Earth and*

Planetary Science Letters 621, 118370. https://doi.org/10.1016/j.epsl.2023.118370

Stolper, E. (1982) The speciation of water in silicate melts. *Geochimica et Cosmochimica Acta* 46, 2609–2620. https://doi.org/10.1016/0016-7037(82)90381-7

Troch, J., Huber, C., Kueter, N., Guillong, M., Ackerson, M., Ulmer, P., Bachmann, O. (2024) The effect of water on alkali trace element diffusion (Li, Rb, Cs) in silicic melts. *Geochimica et Cosmochimica Acta* 365, 101–113. https://doi.org/10.1016/j.gca.2023.11.031

Truckenbrodt, J., Johannes, W. (1999) H_2O loss during piston-cylinder experiments. *American Mineralogist* 84, 1333–1335. https://doi.org/10.2138/am-1999-0909

Wallace, P.J., Plank, T., Bodnar, R.J., Gaetani, G.A., Shea, T. (2021) Olivine-Hosted Melt Inclusions: A Microscopic Perspective on a Complex Magmatic World. *Annual Review of Earth and Planetary Sciences* 49, 465–494. https://doi.org/10.1146/annurev-earth-082420-060506

Watson, E.B. (1979) Diffusion of Cesium Ions in H_2O-Saturated Granitic Melt. *Science* 205, 1259–1260. https://doi.org/10.1126/science.205.4412.1259

Watson, E.B. (1981) Diffusion in magmas at depth in the Earth: The effects of pressure and dissolved H_2O. *Earth and Planetary Science Letters* 52, 291–301. https://doi.org/10.1016/0012-821X(81)90184-9

Watson, E.B., Baker, D.R. (1991) Chemical Diffusion in Magmas: An Overview of Experimental Results and Geochemical Applications. In: Perchuk, L.L., Kushiro, I. (Eds.) *Physical Chemistry of Magmas*. Springer, New York, 120–151. https://doi.org/10.1007/978-1-4612-3128-8_4

Watson, E.B., Cherniak, D.J., Thomas, J.B., Hanchar, J.M., Wirth, R. (2016) Crystal surface integrity and diffusion measurements on Earth and planetary materials. *Earth and Planetary Science Letters* 450, 346–354. https://doi.org/10.1016/j.epsl.2016.06.043

Zhang, Y., Behrens, H. (2000) H_2O diffusion in rhyolitic melts and glasses. *Chemical Geology* 169, 243–262. https://doi.org/10.1016/S0009-2541(99)00231-4

Zhang, Y., Ni, H., Chen, Y. (2010) Diffusion Data in Silicate Melts. *Reviews in Mineralogy and Geochemistry* 72, 311–408. https://doi.org/10.2138/rmg.2010.72.8